

Overcoming bandwidth limitations in space-coiled acoustic metamaterials through inclined perforated plate design

Jixin Liu(刘继鑫), Fengmin Wu(吴丰民), Ting Li(李婷), Junjun Wang(王军军), Xinye Zou(邹欣晔), and Dong Zhang(章东)

Citation: Chin. Phys. B, 2025, 34 (**1**): 014303. DOI: 10.1088/1674-1056/ad8fa2

What follows is a list of articles you may be interested in

Ultra-broadband acoustic ventilation barrier based on multi-cavity resonators

Yu-Wei Xu(许雨薇), Yi-Jun Guan(管义钧), Cheng-Hao Wu(吴成昊), Yong Ge(葛勇), Qiao-Rui Si(司乔瑞), Shou-Qi Yuan(袁寿其), and Hong-Xiang Sun(孙宏祥)

Chin. Phys. B, 2023, 32 (**12**): 124303. DOI: 10.1088/1674-1056/acf5d1

Energy-distributable waterborne acoustic launcher for directional sensing

Tian Yang(杨天), Wenting Gao(高文婷), Shida Fan(范世达), Jie Ren(任捷), and Tianzhi Yang(杨天智)

Chin. Phys. B, 2023, 32 (**12**): 124302. DOI: 10.1088/1674-1056/acf5cf

Theory of complex-coordinate transformation acoustics for non-Hermitian metamaterials

Hao-Xiang Li(李澔翔), Yang Tan(谭杨), Jing Yang(杨京), and Bin Liang(梁彬)

Chin. Phys. B, 2023, 32 (**9**): 094301. DOI: 10.1088/1674-1056/acc3fc

Nonlinear wave propagation in acoustic metamaterials with bilinear nonlinearity

Shiqi Liang(梁诗琪), Jiehui Liu(刘杰惠), Yun Lai(赖耘), and Xiaozhou Liu(刘晓宙)

Chin. Phys. B, 2023, 32 (**4**): 044301. DOI: 10.1088/1674-1056/ac9783

Controlling acoustic orbital angular momentum with artificial structures: From physics to application

Wei Wang(王未), Jingjing Liu(刘京京), Bin Liang (梁彬), and Jianchun Cheng(程建春)

Chin. Phys. B, 2022, 31 (**9**): 094302. DOI: 10.1088/1674-1056/ac7868

Overcoming bandwidth limitations in space-coiled acoustic metamaterials through inclined perforated plate design

Jixin Liu(刘继鑫)[1], Fengmin Wu(吴丰民)[1,3,†], Ting Li(李婷)[1], Junjun Wang(王军军)[1], Xinye Zou(邹欣晔)[2,‡], and Dong Zhang(章东)[1,2,3,§]

[1] *Department of Applied Physics, School of Science, Harbin University of Science and Technology, Harbin* 150080, *China*
[2] *Key Laboratory of Modern Acoustics (MOE), Department of Physics, Collaborative Innovation Center of Advanced Microstructure, Nanjing University, Nanjing* 210093, *China*
[3] *Laboratory of Solid State Microstructures, Nanjing University, Nanjing* 210093, *China*

(Received 3 October 2024; revised manuscript received 4 November 2024; accepted manuscript online 7 November 2024)

Traditional space-coiled acoustic metamaterials have been widely used in the fields of low-frequency sound absorption and noise reduction. However, they have limitations in terms of low-frequency absorption bandwidth, and the weak coupling effect under complex coiled structures also limits their applications. In this work, we introduce the composite structure changing the characteristic impedance of acoustic metamaterials to enhance the coupling effect. Meanwhile, the perforated plates with inclined design instead of traditional partitions greatly improve the sound absorption. The model and method designed in this paper show significant innovation in enhancing low-frequency absorption performance.

Keywords: metamaterials, composite structure, over-damped modes coupling, sound absorption

PACS: 43.35.+d, 43.40.+s, 43.50.+y

DOI: 10.1088/1674-1056/ad8fa2 **CSTR:** 32038.14.CPB.ad8fa2

1. Introduction

Acoustic metamaterials, as a unique type of artificially engineered material, have attracted widespread attention over the past several years.[1–7] Anomalous control of acoustic waves can be achieved by structural design of metamaterials, such as extraordinary reflection,[8] negative refraction,[9] and superlensing.[10,11] Due to the significant importance of sound absorption and noise reduction in everyday life and industrial applications, sound-absorbing acoustic metamaterials have attracted considerable attention,[12–17] especially space-coiled acoustic metamaterials with flexible adjustment and excellent low-frequency sound-absorbing properties.[18–24] Conventional space-coiled acoustic metamaterials with a two-dimensional labyrinth channel design have been widely used in low-frequency sound absorption and noise reduction.[25–30] However, there is still room for further optimization because of its narrow absorption bandwidth and poor multi-unit coupling effect.[31]

On the other hand, the microperforated plates (MPP) have been demonstrated to obtain excellent performances in sound absorption and sound insulation.[32–36] Considering its unique structural construction and sound absorption mechanism, Li and others have achieved the purpose of promoting low-frequency absorption by perforating the surface of space-coiled acoustic metamaterials.[24,26,34] Although this series of methods can better solve the problem of low-frequency absorption, their practices generally remain in the surface design of metamaterials, such as additional perforation design on the surface of space-coiled metamaterials and other structural change methods. In fact, these methods do not fully utilize the internal structural space of metamaterials, so there is still some room for improvement.

In this paper, we propose a composite inclined perforated plate space-coiled acoustic metamaterial (IPP-SCAM) to address the weak coupling issue of space-coiled structures in low-frequency absorption. The structure consists of eight uneven space-coiled structures, each unit is designed to enhance the interaction between structures and overall sound absorption capability. Specifically, replacing the traditional partitions inside the structure by perforated plates with inclined holes, the damping state of the system is change, and the coupling effect between structures is further enhanced. Compared with traditional space-coiled acoustic metamaterials, the designed composite structure has significantly improved the low-frequency absorption and stability. Meanwhile, the experimental results are in good agreement with the numerical results, which proves the reliability of this research design scheme.

†Corresponding author. E-mail: fmwu@hrbust.edu.cn
‡Corresponding author. E-mail: xyzou@nju.edu.cn
§Corresponding author. E-mail: dzhang@nju.edu.cn

© 2025 Chinese Physical Society and IOP Publishing Ltd. All rights, including for text and data mining, AI training, and similar technologies, are reserved.

2. Modeling and theoretical analysis

Traditional perforated plate sound absorption devices are usually composed of a thin plate with holes and a cavity below. However, common adjustment methods mainly include changing the perforation rate, plate thickness, and cavity depth. Here, based on previous research on inclined holes,[22,36] we introduce inclined hole perforated plates into space-coiled acoustic metamaterials to explore the impact on absorption performance and the corresponding physical mechanisms.

The designed structure consists of a perforated plate and an internal cavity, measuring 54 mm×54 mm×52 mm. The relevant parameters for the perforated plate are the hole radius of 1 mm, the perforation rate of 16.7%, and the plate thickness of 2 mm. The inclined holes is introduced by inclining the traditional long straight cylindrical perforations along the vertical to the horizontal, as shown in Fig. 1. For the convenience of subsequent description and calculation, the incline angle is defined as α, and the degree of incline is described by the tangent value $\tan\alpha$. Generally, the larger the value of $\tan\alpha$, the smaller the degree of incline of the perforations.

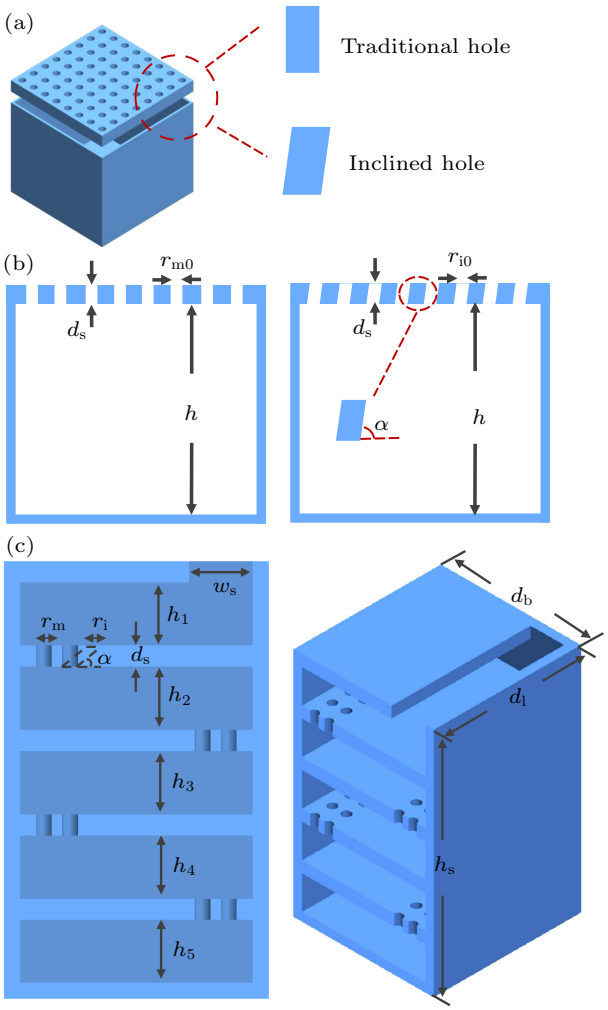


Fig. 1. Structural schematic diagram. (a) Schematic diagram of a microperforated plate model; (b) microperforated plate absorber profile on the left, inclined hole microperforated plate absorber profile on the right; (c) profile diagram and isometric view of IPP-SCAM.

Sound absorption by metamaterials is mainly influenced by the interaction of sound waves with the material structure. The key parameters affecting sound absorption are the acoustic impedance of the material and the boundary conditions set by the geometry of the structure (the size and orientation of the holes). First, the effect of inclined holes on the sound absorption properties of acoustic materials is analyzed and explored. By incorporating geometrical modifications into the classical model of acoustic interactions, we derive expressions for the acoustic impedance and the absorption coefficient, emphasizing the role of inclination in enhancing low-frequency sound absorption.

The inclined hole can be considered as a vertical perforation of the extended path, and the effective perforation length can be expressed as $l = d_s/\sin\alpha$, and its acoustic impedance can be expressed as

$$Z_{\mathrm{IPP}} = \mathrm{j}\omega\rho_0 l\left[1 - \frac{2}{s'\sqrt{-\mathrm{j}}}\frac{\mathrm{J}_1\left(s'\sqrt{-\mathrm{j}}\right)}{\mathrm{J}_0\left(s'\sqrt{-\mathrm{j}}\right)}\right]^{-1}, \tag{1}$$

where ω represents the angular frequency, ρ_0 is the air density, d_s is the perforation length (usually the thickness of the perforated plate), η is the viscosity coefficient, J_0 is the 0th order Bessel function, J_1 is the 1st order Bessel function, $s' = r_{i0}\sqrt{\rho_0\omega/\eta}$ is the inclined hole perforation constant and r_{i0} is the radius of the inclined hole perforation.

Through the transfer matrix method, the sound absorption coefficient of the structure is further calculated. Assuming the upstream and downstream particle velocities in the thin perforated plate are the same, the transfer matrix can be simplified as

$$T_{\mathrm{IPP}} = \begin{bmatrix} 1 & Z_{\mathrm{IPP}} \\ 0 & 1 \end{bmatrix}. \tag{2}$$

On the other hand, the transfer matrix of the cavity behind the plate can be written as

$$T_{\mathrm{c}} = \begin{bmatrix} \cos(k_0 h) & \mathrm{j}Z_0\sin(k_0 h) \\ \dfrac{\mathrm{j}\sin(k_0 h)}{Z_0} & \cos(k_0 h) \end{bmatrix}. \tag{3}$$

Therefore, the overall transfer matrix of a multilayer composite structure can be obtained by multiplying the matrices of the various components in the structure.

$$T_{\mathrm{A}} = T_{\mathrm{IPP}1}T_{\mathrm{c}1}T_{\mathrm{IPP}2}T_{\mathrm{c}2}\cdots T_{\mathrm{IPP}n}T_{\mathrm{c}n} = \begin{bmatrix} T_{\mathrm{A}11} & T_{\mathrm{A}12} \\ T_{\mathrm{A}21} & T_{\mathrm{A}22} \end{bmatrix}. \tag{4}$$

Finally, the sound pressure and particle velocity on the surface of the sound-absorbing body can be written as

$$\begin{bmatrix} p_{\mathrm{i}} \\ U_{\mathrm{i}} \end{bmatrix} = T_{\mathrm{A}}\begin{bmatrix} p_{\mathrm{e}} \\ U_{\mathrm{e}} \end{bmatrix} = \begin{bmatrix} T_{\mathrm{A}11} & T_{\mathrm{A}12} \\ T_{\mathrm{A}21} & T_{\mathrm{A}22} \end{bmatrix}\begin{bmatrix} p_{\mathrm{e}} \\ U_{\mathrm{e}} \end{bmatrix}. \tag{5}$$

Furthermore, the surface acoustic impedance $Z_{\mathrm{s}} = p_{\mathrm{i}}/U_{\mathrm{i}} = T_{\mathrm{A}11}/T_{\mathrm{A}21}$ can be used to obtain the structure's sound

absorption coefficient

$$A = 1 - \left| \frac{Z_s - Z_0}{Z_s + Z_0} \right|^2. \tag{6}$$

The characteristic impedance of air is $Z_0 = \rho_0 c_0$, where c_0 represents the speed of sound propagation in the air.

3. Numerical results and discussion

Figure 2(a) shows the sound absorption of the model at $\tan\alpha = 1$ for temperatures 293 K–313 K. From the figure, it can be seen that the sound absorption coefficient does not change much with increasing temperature and remains at a high level throughout the frequency range, which indicates that the acoustic metamaterial is able to maintain a stable sound absorption performance under different temperature conditions. Figure 2(b) shows the acoustic absorption of the model at different incline angles. As the tangent decreases it brings about longer perforation paths, which promotes low-frequency absorption, but with it comes a sacrifice in low-frequency bandwidth. The subsequent composite structure compensates for this by enhancing the inter-structure coupling.

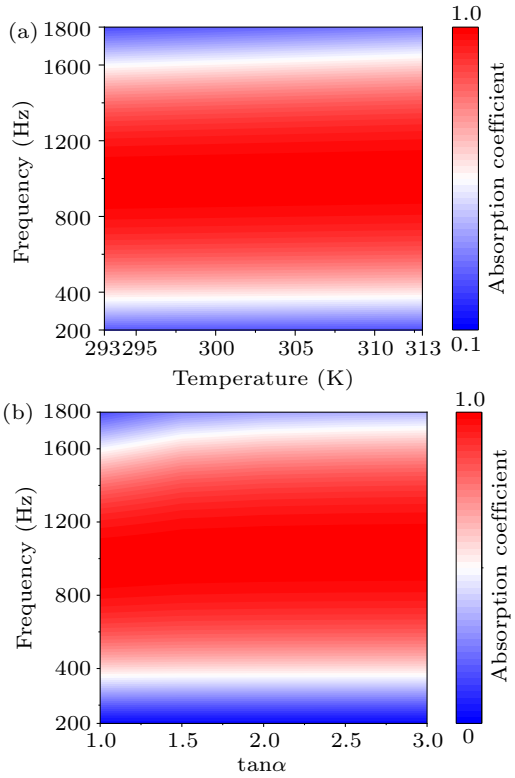


Fig. 2. (a) Acoustic absorption properties at different temperatures when $\tan\alpha = 1$, (b) acoustic performance at different tangents.

Figure 3 illustrates the energy loss modal plots at different tangents, simulated using thermo-viscous acoustics in the finite element simulation software COMSOL Multiphysics 6.0. All models are set to an air domain with a hard sound field boundary, density $\rho_0 = 1.21$ kg/m^3, and sound speed $c_0 = 343$ m/s. In the mode maps of inclined holes with different tangent values (corresponding to the above peak frequencies), the striking red areas marking the high-energy loss at the resonance frequencies are the key locations where energy loss occurs in metamaterials. As the incline angle α of the inclined hole decreases, the greater the energy loss inside the inclined hole. This is attributed to the reduction in the incline angle, which extends the propagation path of the acoustic wave and increases the contact area with the inclined holes, leading to greater thermal viscous losses and improved low-frequency absorption.

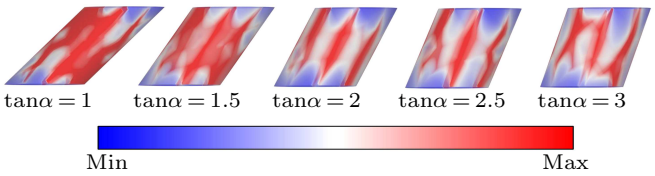


Fig. 3. Modal plots of energy loss at different tangents.

In this study, to further enhance the low-frequency absorption performance of space-coiled acoustic metamaterials (SCAM), The internal partition with a perforated plate was replaced, using smaller holes instead of traditional voids as the propagation channel for sound waves, as shown in Fig. 1(c). Due to the adoption of a multi-layer composite structure, the design of the number of layers in the perforated plate became a key factor. Next, we introduced the inclined hole perforated plate (IPP) for comparison to comprehensively explored its sound absorption performance. Figure 4 illustrates the impact of the number of layers in MPP and inclined hole perforated plates on sound absorption performance and plots the curve of sound absorption coefficients varying with frequency. In the figure, we used a gray dashed line to represent the sound absorption performance of SCAM as a reference to compare the performance of the other three composite perforated plate structures.

After a detailed comparative analysis, it can be found that the sound absorption performance of MPP-SCAM, IPP-SCAM ($\tan\alpha = 3$), and IPP-SCAM ($\tan\alpha = 1$) all shifted towards lower frequencies as the number of perforated plate layers increases. The simulation calculation shows that the absorption frequencies of these three structures are reduced by 19%, 20%, and 26% respectively. This indicates that the low-frequency absorption performance of IPP-SCAM ($\tan\alpha = 1$) is the best, and the increase in the number of composite IPP layers has a positive effect on low-frequency absorption.

The loss factor Q_{loss}^{-1} and leakage factor Q_{leak}^{-1} of the system are calculated based on the coupled mode theory (CMT). The overall coupling pattern of the system can be described using the loss factor Q_{loss}^{-1} and the leakage factor Q_{leak}^{-1}. In general, there exists the mathematical relationship $Q^{-1} = Q_{\text{loss}}^{-1} + Q_{\text{leak}}^{-1}$. For single-port absorbers, the end of the metamaterial is usually a hard acoustic field wall, so there is no transmission of energy through the system. That is the reflection coefficient R at the resonant frequency

can be expressed by the following mathematical relationship $R=\sqrt{\left(Q_{\text{loss}}^{-1}-Q_{\text{leak}}^{-1}\right)^2}/\left(Q_{\text{loss}}^{-1}+Q_{\text{leak}}^{-1}\right)^2$, R denotes the reflection coefficient. Further, the sound absorption coefficient can be calculated as $A=1-|R|^2=4Q_{\text{loss}}^{-1}Q_{\text{leak}}^{-1}/\left(Q_{\text{loss}}^{-1}+Q_{\text{leak}}^{-1}\right)^2$. Subsequently, the loss factor Q_{loss}^{-1} and the leakage factor Q_{leak}^{-1} of the system can be calculated from the relationship between the absorption coefficient curve A, the peak absorption frequency f_{r}, and the half-peak width Δf of the resonance frequency. Then, the coupling pattern of the system is then determined by the size relationship between the two.

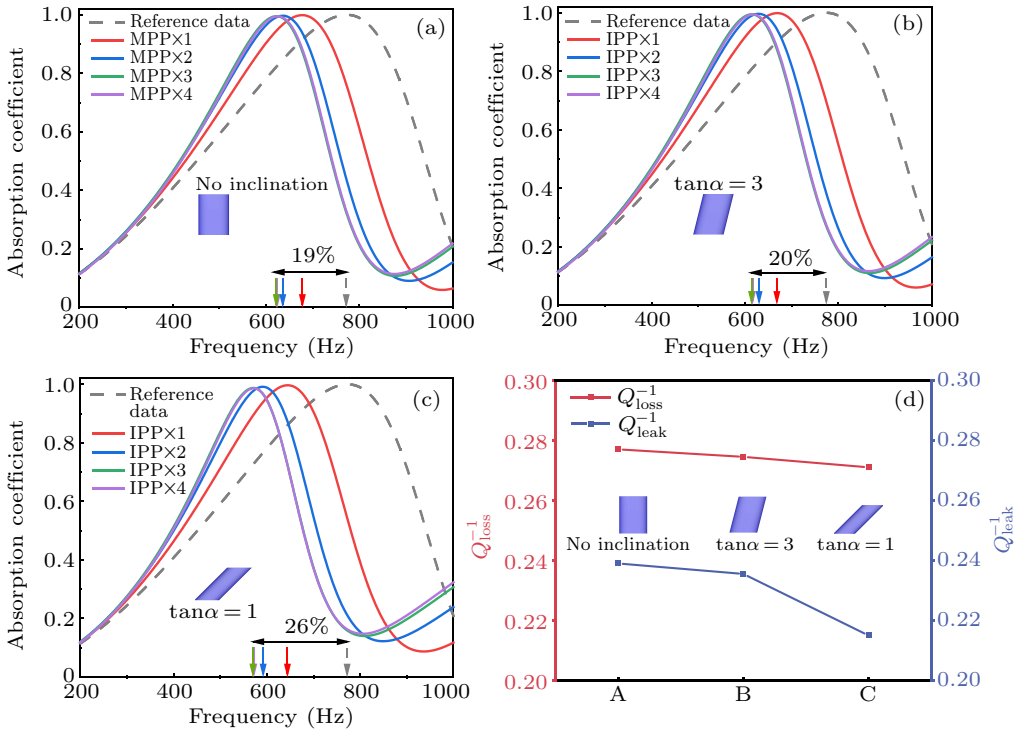


Fig. 4. Effect of the number of layers of MPP and IPP on sound absorption performance. (a) The influence of the number of MPP layers on acoustic absorption performance. The effect of the number of IPP layers on sound absorption performance at (b) $\tan\alpha=3$ and (c) $\tan\alpha=1$. (d) Q_{loss}^{-1} and Q_{leak}^{-1} for models A (MPP-SCAM), B (IPP-SCAM ($\tan\alpha=3$)), C (IPP-SCAM ($\tan\alpha=1$)).

Where I, II, and III denote the MPP-SCAM, IPP-SCAM ($\tan\alpha=3$), and IPP-SCAM ($\tan\alpha=1$) replacement four-layer spacer structures, respectively. After calculating the loss factor Q_{loss}^{-1} and leakage factor Q_{leak}^{-1} of the system, the damping state of the system can be determined from the magnitude relationship between Q_{loss}^{-1} and Q_{leak}^{-1}, as shown in Fig. 4(d). When the two points of the values of Q_{loss}^{-1} and Q_{leak}^{-1} coincide, it means that the system is in the impedance matching state. And the farther away the two points are from each other indicates that the impedance is more mismatched. According to Fig. 4(d), it can be clearly observed that the difference between the loss factor Q_{loss}^{-1} and the leakage factor Q_{leak}^{-1} of I, II, and III is getting bigger and bigger and always in the relationship of $Q_{\text{loss}}^{-1}>Q_{\text{leak}}^{-1}$, which indicates that the increase of incline angle of inclined hole perforated plate changes the characteristic impedance of the system, and the system is gradually transformed to the over-damped state. Therefore, the coupling effect between the two is increasingly strong.

To thoroughly analyze the reasons of promoting low-frequency absorption, the real and imaginary parts of impedance are calculated to assess the damping state of the system, as shown in Fig. 5. When $\text{Re}\left(Z_{\text{s}}/Z_0\right)=1$, it represents complete consumption of the incident acoustic energy. Figures 5(a)–5(c) show that the real parts of the impedance for MPP-SCAM, IPP-SCAM ($\tan\alpha=3$), and IPP-SCAM ($\tan\alpha=1$) structures are slightly greater than one at their resonant frequencies, and with an increase in the incline angle, the real part of the impedance also increases. Such variations indicate that a larger incline angle enhances the system's energy dissipation capability but also gradually leads to impedance mismatch, transitioning from an impedance-matched state to an over-damped state. In an over-damped system, the system could rapidly decay the oscillations of incident sound waves, minimizing the energy of reflected sound waves, thereby improving energy absorption efficiency and enhancing inter-unit coupling.

The acoustic responses such as sound absorption coefficient and sound pressure of SCAM and IPP-SCAM are also simulated. The designed IPP-SCAM broadband absorber consists of eight carefully designed independent units. The main parameters include an incident port width $w_{\text{s}}=6$ mm, a inclined hole angle $\alpha=63.435°$, a plate thickness $d_{\text{s}}=2$ mm, an inclined hole radius $r_{\text{i}}=0.75$ mm, a sub-unit length $d_l=47$ mm, a width $d_{\text{b}}=22$ mm, and a height $h_{\text{s}}=40$ mm.

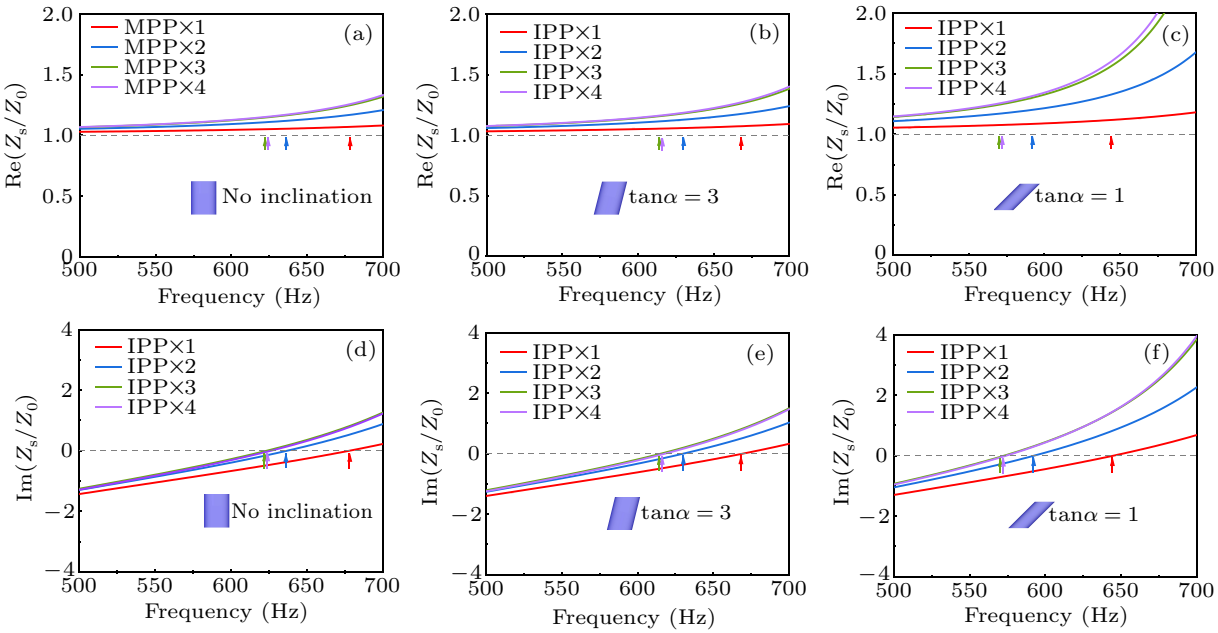


Fig. 5. Characteristic impedance of MPP and IPP related layers: (a) real part and (d) imaginary part of MPP impedance at different layers, (b) real part and (e) imaginary part of MPP impedance at different layers at tan $\alpha = 3$, (c) real part and (f) imaginary part of MPP impedance at different layers at tan $\alpha = 1$.

To validate the conclusions proposed above, finite element simulations are conducted for calculation. The relative surface acoustic pressure $|P|/P_0$ and particle vibration velocity are extracted to simulate the strong coupling of the multi-unit structure IPP-SCAM as shown in Fig. 6(a). Three characteristic modes I, II, III are selected for analysis, corresponding to the characteristic modalities at 494 Hz, 550 Hz, and 620 Hz respectively. In the three modal plots, the blue area represents the lower sound pressure, the red area represents the higher sound pressure, and the arrows indicate the propagation direction of the sound wave and the magnitude of the sound velocity. The increase in the speed of sound as well as the diversity of propagation directions indicates that the sound waves interact with each other in different units and the energy transfer is more efficient. It can be clearly observed that multiple units participate in absorption at each characteristic frequency, rather than a discrete single action. In this way, the material can provide maximum sound absorption performance at different frequency points.

To conduct a detailed acoustic performance evaluation of the IPP-SCAM broadband sound absorber, the assembled sample was placed in the material acoustic testing system as shown in Fig. 6(b). The sample was measured multiple times by rotating it. Manufacturing was done using 3D printing technology, using resin as the raw material, with the following properties: density 1.12 g/cm^3, modulus of elasticity 2589 MPa, Poisson's ratio 0.42, heat deflection temperature 58 °C, strain at break 11%, yield strain 3.4%. The acoustic test system selected was the BSWA F100 impedance tube test system at 20 °C for testing, as shown in Fig. 6(b). A total of multi-channel data acquisition instrument MC3242A, measurement power amplifier PA50, sound-absorbing impedance tube F100, microphone MPA416, and so on. It meets the test standards GB/T 18696.2, GB/J 88, ISO 10534-2, ASTM E1050-12.

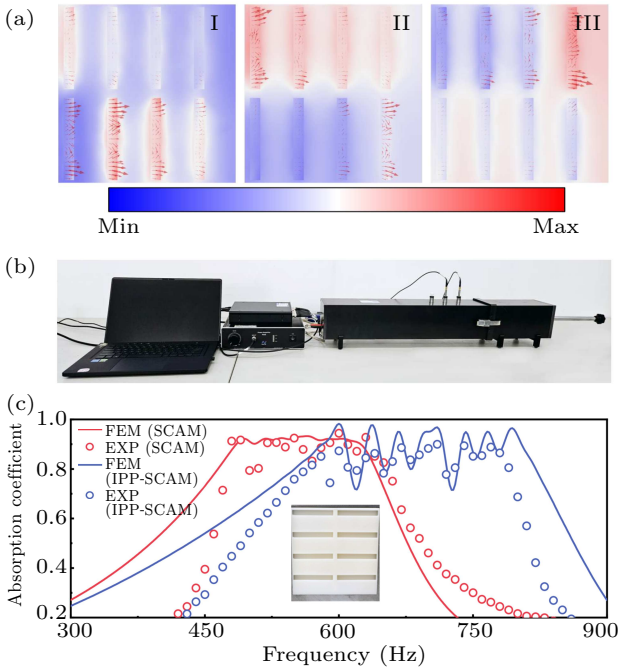


Fig. 6. Testing and results: (a) IPP-SCAM modal maps of surface coupling at different resonance frequencies, (b) acoustic test systems, (c) simulation and experimental results.

As shown in Fig. 6(c), the experimental data and simulation data have good consistency, and there are some differences possibly due to the errors generated during the sample manufacturing process. The designed structure IPP-SCAM can achieve an absorption coefficient of over 0.9 within the frequency range of 486 Hz–623 Hz. The broadband absorption effect of IPP-SCAM benefits from the coupling action of

eight over-damped state absorption units, which significantly improves both low-frequency absorption and structural coupling compared to traditional SCAM.

4. Conclusions

In conclusion, we thoroughly discuss the impact on sound absorption performance of acoustic metamaterial after replacing the traditional partitions with an inclined hole perforated plate. Through theoretical derivation, finite element simulation, and experimental testing, it has been verified that the change in its impedance mode brings stronger coupling effects between different structures of the system, and the optimized structure has significantly improved low-frequency absorption performance. Notably, the optimized IPP-SCAM broadband absorber can achieve a sound absorption coefficient of over 0.9 within the frequency range of 486 Hz–623 Hz, which is significantly better than the traditional SCAM, significantly improving the low-frequency broadband absorption effect and absorption stability.

Acknowledgements

Project supported by the National Key Research and Development Program of China (Grant No. 2022YFB3204303), the National Natural Science Foundation of China (Grant No. 11934009), the Fundamental Research Funds for the Central Universities (Grant No. 020414380195), and the Foundation of State Key Laboratory of Ultrasound in Medicine and Engineering (Grant No. 2022KFKT021).

References

[1] Li J, Wen X and Sheng P 2021 *J. Appl. Phys.* **129** 171103
[2] Qu S and Shen P 2022 *Phys. Rev. Appl.* **17** 047001
[3] Guo J, Fang Y, Qu R and Zhang X 2023 *Mater. Today* **66** 321
[4] Zhang J, Hu B and Wang S 2023 *Appl. Phys. Lett.* **123** 010502
[5] Wang B and Huang J P 2022 *Chin. Phys. B* **31** 098101
[6] Liang S Q, Liu J H, Lai Y and Liu X Z 2023 *Chin. Phys. B* **32** 044301
[7] Yang Y, Ma D K and Zhang L F 2023 *Chin. Phys. Lett.* **40** 124401
[8] Song G Y, Cheng Q, Cui T J and Jing Y 2018 *Phys. Rev. Mater.* **2** 065201
[9] He H, Qiu C, Ye L, Cai X, Fan X, Ke M, Zhang F and Liu Z 2018 *Nature* **560** 61
[10] Lin Z, Zhang Y, Wang K W and Tol S 2022 *Appl. Phys. Lett.* **121** 201703
[11] Hu C, Xue S, Yin Y, Hao Z, Zhou Y and Chen H 2022 *Appl. Phys. Lett.* **120** 192202
[12] Shen L, Zhu Y F, Mao F L, Gao S Y, Su Z H, Luo Z T, Zhang H and Assouar B 2021 *Phys. Rev. Appl.* **16** 064057
[13] Li Y, Lin Y and Peng Y 2022 *J. Appl. Phys.* **132** 115104
[14] Xie S H, *et al.* 2020 *Chin. Phys. Lett.* **37** 054301
[15] Zhu Y, Long H, Liu C, Zhang H, Cheng Y and Liu X 2022 *Appl. Phys. Lett.* **120** 141701
[16] Liu L, Xie L X, Huang W, Zhang X J, Lu M H and Chen Y F 2022 *Appl. Phys. Lett.* **120** 251701
[17] Liu C, Wang H, Liang B, Cheng J C and Lai Y 2022 *Appl. Phys. Lett.* **120** 231702
[18] Du J, Luo Y, Zhao X, Sun X, Song Y and Hu X 2021 *Sci. Rep.* **11** 5829
[19] Xie Y, Wang W, Chen H, Konneker A, Popa B I and Cummer S A 2014 *Nat. Commun.* **5** 5553
[20] Liu C, Shi J, Zhao W, Zhou X, Ma C, Peng R, Wang M, Hang Z H, Liu X, Christensen J, Fang N X and Lai Y 2021 *Phys. Rev. Lett.* **127** 084301
[21] Liang Z and Li J 2012 *Phys. Rev. Lett.* **108** 114301
[22] Zhang C and Hu X 2016 *Phys. Rev. Appl.* **6** 064205
[23] Liu Y, Zeng X, Ren S, Sun W, Zeng Y, Wang H and Lei Y 2023 *J. Appl. Phys.* **134** 085104
[24] Abrahams M P, Oudich M, Revalor Y, Vukadinovic N and Assouar B 2024 *Appl. Phys. Lett.* **124** 151702
[25] Ryoo H and Jeon W 2018 *Appl. Phys. Lett.* **113** 121903
[26] Li Y and Assouar B M 2016 *Appl. Phys. Lett.* **108** 063502
[27] Huang S, Fang X, Wang X, Assouar B, Cheng Q and Li Y 2018 *Appl. Phys. Lett.* **113** 233501
[28] Shen Y, Yang Y, Guo X, Shen Y and Zhang D 2019 *Appl. Phys. Lett.* **114** 083501
[29] Pavan G and Singh S 2024 *J. Acoust. Soc. Am.* **155** 496
[30] Xu Q, Qiao J, Zhang G and Li L 2023 *J. Appl. Phys.* **133** 075106
[31] Günay M, Biçer A, Korozlu N and Cicek A 2023 *Appl. Phys. Lett.* **123** 092201
[32] Carbajo J, Ghaffari Mosanenzadeh S, Kim S and Fang N X 2020 *Appl. Acoust.* **169** 107496
[33] Jiang C S, Li X H, Cheng W Y, Luo Y and Xing T 2020 *Appl. Acoust.* **157** 106998
[34] Liu Y, Ren S, Sun W, Lei Y, Wang H and Zeng X 2021 *Appl. Phys. Lett.* **119** 101901
[35] Shao C, Zhu Y, Long H, Liu C, Cheng Y and Liu X 2022 *Appl. Phys. Lett.* **120** 083504
[36] Carbajo J, Ghaffari Mosanenzadeh S, Kim S and Fang N X 2020 *Appl. Phys. Lett.* **116** 054101